Inorganic Chemistry

Article

pubs.acs.org/IC

A QMCF-MD Investigation of the Structure and Dynamics of Ce^{4+} in Aqueous Solution

Oliver M. D. Lutz, Thomas S. Hofer,* Bernhard R. Randolf, Alexander K. H. Weiss, and Bernd M. Rode

Theoretical Chemistry Division, Institute of General, Inorganic and Theoretical Chemistry, University of Innsbruck, Innrain 80-82, A-6020 Innsbruck, Austria

Supporting Information

ABSTRACT: A quantum-mechanical charge-field molecular dynamics simulation has been performed for a tetravalent Ce ion in aqueous solution. In this framework, the complete first and second hydration spheres are treated by ab initio quantum mechanics supplemented by an electrostatic embedding technique, making the construction of non-Coulombic solute−solvent potentials unnecessary. During the 10 ps of simulation time, the structural aspects of the solution were analyzed by various methods. Experimental results such as the mean Ce−O bond distance and the predicted first-shell coordination number were compared to the results obtained from the simulation resolving some ambiguities in the literature. The dynamics of the system were characterized by mean ligand residence times and frequency/force constant calculations. Furthermore, Ce−O and Ce−H angular radial distribution plots were employed, yielding deeper insight into the structural and dynamical aspects of the system.

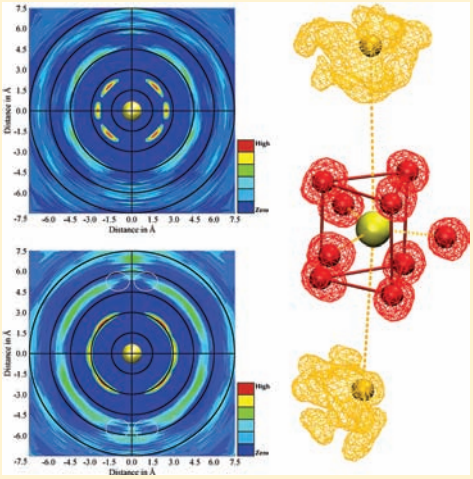

1. INTRODUCTION

Cerium is the second element of the rare-earth metals. The tetravalent ion has many important applications, especially in its form as an oxide (CeO_2). It is, together with transition-metal oxides such as TiO_2, used as a colorizing agent in the glass manufacturing industry. The oxide can be employed as a decolorizing agent, and it can be used for selective UV absorption.[1] It is being used in the optical industry as well as in the jewelry and watch industry as a high-performance polishing compound.[1] An older, but still important, application is the use as an active component in incandescent gas lamp mantles such as the Welsbach mantle, where CeO_2 is used together with lanthanum, magnesium, thorium, or yttrium oxides. The ion has been used extensively for a long time as a volumetric oxidizing agent in quantitative redox analysis,[1] awakening interest in improving the understanding of the ion's hydration. Besides the aforementioned applications, the utilization of cerium in catalysis,[2] its characterstics in a biochemical context,[3] and electrochemical applications in fuel-cell electrodes[4] are investigations motivating the examination of the tetravalent cerium on a computational basis. The study of aqueous Ce^{4+} via a quantum-chemical simulation approach was partly motivated by an extended X-ray absorption fine structure (EXAFS) experiment published by Solera et al.[5] reporting 12-fold coordination for the first hydration sphere, which appears highly unlikely. Given that Ce^{4+} is easily photoreduced to Ce^{3+}, the 9-fold-coordinated first hydration shell reported by Sham[6] seems likely because he assured, by characterizing the solutions adjacent to the X-ray beamline, that the ions under investigation were indeed tetravalent. Furthermore, Sham's approach is based on the utilization of nitrate salts, whereas Solera et al.[5] used the corresponding chloride salts for sample preparation: the works by Kanno and Hiraishi[7] suggest, from their Raman scattering experiments, that the usage of nitrate salts is preferred over the corresponding chloride species when investigating the hydration of rare-earth ions. The experimentally determined mean first-shell Ce−O distance differs as well: Solera et al.[5] suggested 2.53 Å, whereas Sham's analysis[6] yielded 2.42 Å. It is worth mentioning, however, that the bond lengths reported by these two experiments in solution are longer than the sum of the ionic radius of the tetravalent cerium[8] and the radii of coordinated water molecules (~1.34 Å).[9]

So far, no theoretical approach has been undertaken toward determining the structural and dynamical properties of the Ce^{4+} ion in aqueous solution. Given the availability of today's powerful computing facilities, it appeared promising to rectify the aforementioned ambiguities in the literature with a high-level method, thereby calculating the two innermost hydration spheres at the Hartree−Fock (HF) double-ζ quantum-mechanical (QM) level and the bulk region via the BJH-CF2 water model.[10,11] The quality of the quantum-mechanical charge-field molecular dynamics (QMCF-MD) approach has

Received: February 21, 2012
Published: May 31, 2012

   dx.doi.org/10.1021/ic300385s | *Inorg. Chem.* 2012, 51, 6746−6752

been validated by various studies - structural and dynamical properties are either well in agreement with experimental data or are produced with higher accuracy than experimentally available.[12−16]

2. METHODS

2.1. Simulation Method. The employed QMCF-MD approach,[17−19] as well as the conventional QM/molecular mechanics (MM) ansatz[20,21] and ONIOM approaches,[22,23] is based on a partitioning of the simulation box, where the chemically most relevant region surrounding the central species is treated quantum mechanically, while the outer region, in this case containing only water molecules, is treated classically. The QMCF method is extended by means of splitting the QM region into two subregions, the core and layer zones, together occupying a larger part of the box space compared to regular QM/MM simulations.[17−19] This enables a distinct treatment of both the first and second hydration shells, on the one hand, and a more accurate treatment of the system in general, given the larger quantum mechanically treated surroundings of the solute, on the other hand. This implies, however, a significantly increased computational demand: the employed 8 CPU core platform enabled simulation loop times of approximately 200 s per 0.2 fs MD time step. The construction of solute−solvent potentials is a difficult and time-consuming task especially for strongly polarizing ions such as Ce^{4+}; the QMCF ansatz, however, elegantly avoids this problem because of the large QM-treated region[17−19] employed. The fact that non-Coulombic interactions between molecules located inside the core and MM regions become negligible makes the construction of solute−solvent potentials unnecessary. The use of solvent−solvent potentials to compute the interaction within the MM region as well as between MM and QM atoms in the layer region is realized via established potential models for the description of the solvent such as the flexible BJH-CF2 water model,[10,11] which enables explicit hydrogen movements. The forces in the different regions are evaluated as follows:

$$\vec{F}_J^{\,\mathrm{core}} = \vec{F}_J^{\,\mathrm{QM}} \tag{1}$$

$$\vec{F}_J^{\,\mathrm{layer}} = \vec{F}_J^{\,\mathrm{QM}} + \sum_{I=1}^{M} \vec{F}_{IJ}^{\,\mathrm{BJHnC}} \tag{2}$$

$$\vec{F}_J^{\,\mathrm{MM}} = \sum_{\substack{I=1 \\ I\neq J}}^{M} \vec{F}_{IJ}^{\,\mathrm{BJH}} + \sum_{I=1}^{N_1+N_2} \frac{q_I^{\mathrm{QM}} q_J^{\mathrm{MM}}}{\vec{r}_{IJ}^{\,2}} + \sum_{I=1}^{N_2} \vec{F}_{IJ}^{\,\mathrm{BJHnC}} \tag{3}$$

$\vec{F}_J^{\,\mathrm{core}}$ corresponds to the QM forces acting on a particle J located within the innermost region, the core zone, and $\vec{F}_J^{\,\mathrm{layer}}$ reflects the forces acting on a particle J located in the solvation layer. The non-Coulombic interactions of atoms in the solvation layer with MM particles obtained from the BJH-CF2 water model[10,11] are taken into account as well because this layer is located in the immediate neighborhood of the MM region.

The forces acting on the MM particles are extended via inclusion of the Coulombic forces exerted by the core-zone (N_1) and layer-zone (N_2) particles, whose charges are obtained by Mulliken[24,25] population analysis, as well as the non-Coulombic forces exerted by the layer-zone particles. The employment of Mulliken population analysis for this purpose has proven to be most compatible with the BJH-CF2 water model[26] compared to other schemes such as natural bond orbital[27] and Löwdin[28] population analyses. The influence of the MM charges on the QM region is included via a perturbational term of the core Hamiltonian, where M indicates the number of MM particles and q_J corresponds to the respective partial charge (eqs 4 and 5).

$$\hat{H}_{\mathrm{CF}} = \hat{H}_{\mathrm{HF}} + \hat{V}' \tag{4}$$

$$\hat{V}' = \sum_{J=1}^{M} \frac{q_J}{r_{IJ}} \tag{5}$$

The QMCF-MD methodology is similar in spirit to the well-known ONIOM approach developed by Morokuma and co-workers[22] and employs the electrostatic embedding technique to improve the description of the high-level region.[19] The main advantage of the QMCF-MD formalism is the possibility of employing point-charge embedding in a periodic environment.[17]

It is important to ensure smooth particle migration from the QM to the MM region and vice versa. This is achieved by defining a smoothing zone[19] having a typical width of 0.2 Å (eq 6)

$$\vec{F}_J^{\,\mathrm{smoothing}} = S(r)\,(\vec{F}_J^{\,\mathrm{layer}} - \vec{F}_J^{\,\mathrm{MM}}) + \vec{F}_J^{\,\mathrm{MM}} \tag{6}$$

where the smoothing factor $S(r)$ is

$$S(r) = 1, \quad \forall\ \{r \le r_1\} \tag{7}$$

$$S(r) = \frac{(r_0^{\,2} - r^2)^2 (r_0^{\,2} + 2r^2 - 3r_1^{\,2})}{(r_0^{\,2} - r_1^{\,2})^3}, \quad \forall\ \{r_1 < r \le r_0\} \tag{8}$$

$$S(r) = 0, \quad \forall\ \{r > r_0\} \tag{9}$$

r is the distance of a solvent molecule's center from the QM center, r_0 the QM radius, and r_1 the inner border of the smoothing zone.

Another important consideration is the assignment of proper basis sets. For O and H atoms, Dunning double-ζ basis sets with polarizing functions[29] were employed because they have been successfully employed in previous simulation studies. For the Ce ion, a number of available basis sets (ANO-RCC,[30] SBKJC ECP,[31] WTBS,[32,33] and Stuttgart RSC ECPs[34,35]) reported in the EMSL database[36,37] were assessed by performing gas-phase cluster calculations of $[Ce(H_2O)_n]^{4+}$. The optimizations were carried out with the *Gaussian 09* software package.[38] The SBKJC basis set was chosen for the QMCF simulation because of the structural results being in good agreement with reported EXAFS data[6] (see the Supporting Information), the feasible computational effort involved, and the balanced size compared to the basis assigned to the O and H atoms. Either the other basis sets were too demanding for the simulation, resulting in unmanageable computation time, or they did not deliver reasonable data, as was the case for the CRENBL basis set,[39] which delivered unconvincing energies for the Ce ion (i.e., $-2400E_h$). As expected for a strongly polarizing system like Ce^{4+}, electron correlation contributions are rather minor for energies and the HF optimized bond lengths differ neglegibly from the other two investigated methods [Moller−Plesset (MP/2) and coupled cluster with single and double excitation (CCSD)]; for details, reference is made to the exemplary supporting data. The negligible contribution of electron correlation is further confirmed by the data published for trivalent lanthanoid ions by Kuta and Clark in 2010.[40] Significant contribution to the total energy was only found for lanthanoid ions with two to five unpaired electrons (i.e., Pr^{3+}, Nd^{3+}, Pm^{3+}, Sm^{3+}, and other higher lanthanoids). Thus, and because of the fact that MP/2- and CCSD-based QMCF-MD simulations are computationally too demanding for the studied system size, the HF method was chosen for the simulation.

2.2. Structural Evaluation. Besides ordinary radial distribution functions (RDFs) and angular distribution functions (ADF), local-density-corrected three-body distribution functions[41] were calculated in order to obtain information about the solvent structure in a given solvation shell. This distribution function is formulated as

$$f_{\mathrm{O-X-O}}^{(3)}(s, r, s) = \frac{\langle \bar{n}(s, r, s) \rangle}{8\pi^2 N_X \rho_{\mathrm{shell}}^{\,2} r s^2 \Delta s^2 \Delta r} \tag{10}$$

where N_X denotes the number of species X (in this case, Ce^{4+}) and $\langle \bar{n}(s,r,s) \rangle$ corresponds to the average number of O−X−O triples with X−O distances lying in the range of $s \pm \Delta s/2$. The resulting shape of the function can be compared to ordinary O−O pair distribution functions resembling the structural arragement of undisturbed water, thus allowing for the straightforward identification of a possible solute influence. ρ_{shell} defines the average shell density and is given by the equation

dx.doi.org/10.1021/ic300385s | Inorg. Chem. 2012, 51, 6746−6752

$$\rho_{\text{shell}} = \sqrt{\frac{N_{\text{shell}}(N_{\text{shell}} - 1)}{V_{\text{shell}}^{\ 2}}} \tag{11}$$

In addition, the angular radial distributions (ARDs) of water molecules were computed, yielding detailed information on the structural properties of the hydrate. The idea behind the ARD analysis relies on an angular-weighed RDF calculation: a plane is defined (in this case, by the three capping O atoms and the central ion; Figure 5c) in order to create a normal vector originating from the plane center (i.e., the ion). Prior to the RDF calculations, cones, based in the normal vector, are defined at given increments (i.e., 15°), serving as boundaries for the aforementioned calculations, thus yielding exact ligand localization schemes within a certain time frame.

2.3. Evaluation of Dynamics. To study the dynamical properties of the hydrate, the mean ligand residence times (MRTs) in a given shell were calculated via a direct method:[42]

$$\tau^{0.5} = \frac{t_{\text{sim}}\text{CN}_{\text{avg}}}{N_{\text{ex}}^{\ 0.5}} \tag{12}$$

where t_{sim} is the simulation time and CN_{avg} indicates the average number of particles in the respective shell. The number of registered exchanges with a minimum ligand displacement time of 0.5 ps is given by $N_{\text{ex}}^{\ 0.5}$. The time span of 0.5 ps corresponds to the mean lifetime of a hydrogen bond in water.[43] An important statistical value is the R_{ex} value (eq 13), which indicates the average number of required attempts until a successful exchange event takes place:

$$R_{\text{ex}} = \frac{N_{\text{ex}}^{\ 0.0}}{N_{\text{ex}}^{\ 0.5}} \tag{13}$$

In addition, the vibrational spectrum of the Ce−O motion was obtained via velocity autocorrelation functions

$$C(t) = \frac{\sum_I^{N_t}\sum_J^{N}\vec{v}_J(t_I)\,\vec{v}_J(t_I + t)}{\sum_I^{N_t}\sum_J^{N}\vec{v}_J(t_I)\,\vec{v}_J(t_I)} \tag{14}$$

where N is the number of particles, N_t denotes the number of time origins t_I, and $\vec{v}_J$ indicates a given velocity component of particle J. The power spectrum was calculated via Fourier transformation using a correlation length of 2.0 ps with 2000 averaged time origins. It should be mentioned that HF-obtained frequencies quite constantly deliver a systematic error resulting from the neglected electron correlation contribution and the in vacuo environment. Thus, a factor of 0.89 should be applied to scale all frequencies,[44,45] at least for intramolecular vibrations. However, for this simulation, this correction factor was not applied because of the negligible contribution of the electron correlation and because of the fact that the simulation provides an aqueous environment at ambient conditions. The force constant k was calculated by eq 15:

$$k = 4\pi^2\mu(\tilde{\nu}c)^2 \tag{15}$$

where μ is the reduced mass, $\tilde{\nu}$ is the wavenumber, and c is the speed of light.

2.4. Simulation Protocol. For this particular simulation, a cubic box containing one Ce^{4+} ion and 1000 water molecules with a side length of 31.15 Å was used, corresponding to a ∼0.05 M concentration. The radius of the core zone was set to 3.0 Å and that of the layer zone to 5.7 Å. The simulation was performed in the NVT ensemble, and the temperature of 298.15 K was maintained by the Berendsen weak-coupling algorithm with a relaxation time of 0.1 ps.[46] The system's density was kept at the density of pure water at room temperature (0.997 g/cm^3). An Adams−Bashforth predictor−corrector algorithm was used to integrate the equations of motion with a time step of 0.2 fs. In order to correct the cutoff applied to the long-range electrostatic interactions of 15.0 Å, the reaction-field method was employed.[47] As a starting geometry, the geometry of a previous QMCF-MD simulation of Zr^{4+} in aqueous solution was employed:[48] the simulation box was equlibrated for 2 ps, heated, and finally reequilibrated for 2 ps at ambient conditions to ensure the complete loss of structural ordering from the previous simulation. The sampling period was carried out for 10 ps. Similar to the case of geometry optimizations, the QM part of the simulation was computed with the *Gaussian 09* software package.[38]

3. RESULTS AND DISCUSSION

Ce^{4+} in aqueous solution proved to be very stable already during the first picoseconds of the simulation. Even during the heating period, no hydrolysis reactions occurred and the system remained stable over the whole 10 ps of sampling.

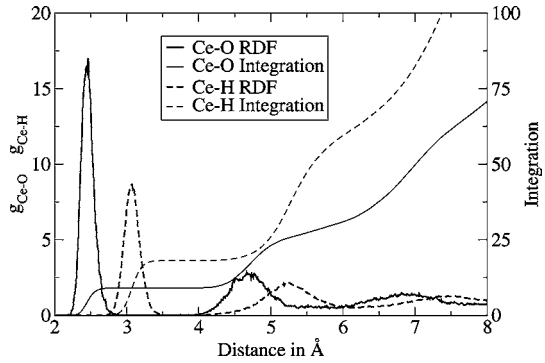

Figure 1. Ce−O (solid line) and Ce−H (dashed line) RDFs and their running integration numbers.

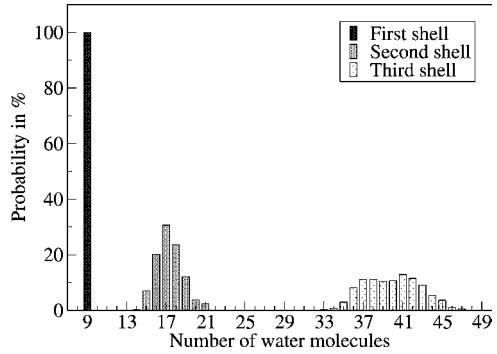

Figure 2. CNDs for the first, second, and third hydration spheres of the hydrated Ce^{4+} ion.

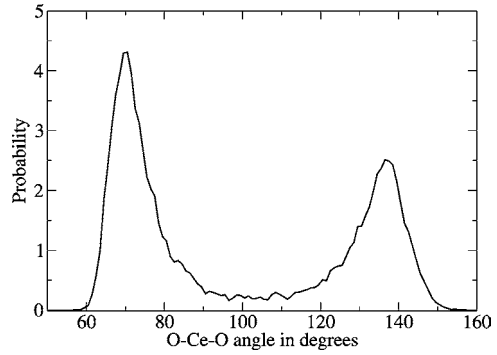

Figure 3. O−Ce−O ADF within the first hydration shell.

3.1. Structural Aspects. *3.1.1. RDFs and Coordination Number Distribution (CND).* Figure 1 shows the Ce−O and Ce−H RDFs and their running integration numbers. Ce^{IV} forms two well-defined hydration spheres, the first one being very stable (no water exchanges were observed along the simulation trajectory). Orientation of the solvent molecules

dx.doi.org/10.1021/ic300385s | *Inorg. Chem.* 2012, 51, 6746−6752

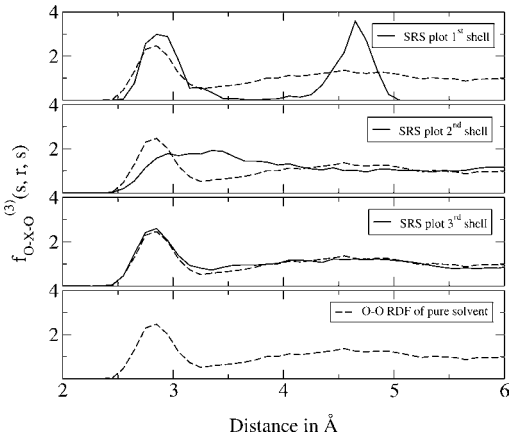

Figure 4. Local-density-corrected three-body distribution functions for the first, second, and third shells of hydration. An overlay of the O−O pair distribution function for pure solvent (dashed line) is given for comparison.[57]

Table 1. Peak Maxima of the Ion−O Stretching Frequencies (Q_{ion-O}) and Corresponding Force Constants (k_{ion-O})

ion	Q_{ion-O}(cm^{-1})	k_{ion-O} (N m^{-1})
$Ce^{4+}_{this\ work}$	420	149
Ce^{4+}_{exp} [6,7]	408	141
Al^{3+} [26]	560	194
Zr^{4+} [48]	484	188
Be^{2+} [56]	734	182

Table 2. Second-Shell MRTs and R_{ex} Values for Various Polarizing Ions in Aqueous Solution

ion	MRT (ps)	R_{ex}
$Ce^{4+}_{this\ work}$	6.0	8.5
U^{4+} [15]	8.1	5.9
Al^{3+} [26]	26.4	15
Zr^{4+} [48]	5.5	6.8
Be^{2+} [56]	4.8	10.0
H_2O [57]	1.7	11.2

even beyond the second hydration shell can be observed from the ill-defined peak between 6.0 and 7.5 Å (Figure 1), indicating the formation of a weak third hydration sphere and thus characterizing the ion as being of a strongly polarizing nature. The two observed inner-shell maxima for the Ce−O and Ce−H distributions are located at 2.44 and 3.07 Å for the first hydration sphere, respectively. For the second hydration layer, values of 4.71 and 5.23 Å were found. The mean first-shell Ce−O distance of 2.44 Å is in excellent agreement with that in Sham's work[6] (2.42 Å); the difference of 0.09 Å between the simulation and Solera's experiment[5] can be attributed to the differences in sample preparation (utilization of chloride salts)[5] compared to Sham's experiment (utilization of nitrate salts)[6] as well as to the different solute concentrations. Furthermore, Sham assured that more than 99.9% of the Ce ions in the solution specimen under investigation were in the Ce^{4+} oxidation state.

The CNDs of the first, second, and third shells are depicted in Figure 2. A stable 9-fold coordination is observed for the first hydration sphere, and no water exchange reactions took place during the simulation time of 10 ps. These observations are in agreement with the findings of Sham, who concluded a "well-defined first-coordination sphere of water",[6] whereas the 12-fold coordination reported by Solera et al.[5] is contradicted by the simulation's outcome. Although Th^{4+} has an electronic configuration significantly different from that of Ce^{4+}, these ions share similar structural properties. Two studies of tetravalent thorium in an aqueous environment presenting quantum-chemical cluster optimizations and classical MD simulations yielded data similar to those observed in the case of Ce^{4+}.[49,50] The nine water molecules resembling the first hydration sphere form either a tricapped trigonal-prismatic or a capped square-antiprismatic structure,[49] which is in agreement with the observed structure of the Ce^{4+} hydrate, as is discussed in section 3.2. Also, the mean second-shell coordination number of 18.9[49] or 17−18[50] water molecules is very similar to the value for Ce^{4+}, which was computed as 17.4. An ill-defined third hydration sphere, as was reported for the Th^{4+} hydrate,[49,50] was also observed in this simulation with an average coordination number of 39.9 water molecules. The resulting mean first-shell Th^{4+}−O bond lengths of 2.45 Å reported by Yang et al.[49] and Réal et al.[50] are in excellent agreement with three published EXAFS experiments[51−53] and thus indicate further similarities with Ce^{4+}. Trivalent lanthanoid ions often resemble properties similar to those of the corresponding tetravalent species. This becomes evident when the simulation outcome is compared with the works by Dinescu and Clark,[54] who concluded the same two structural motifs (trigonal-prismatic and square-antiprismatic hydrates) for Ce^{3+} as those observed during the simulation of Ce^{4+}. The reported mean ion−O bond length is slightly larger in the case of Ce^{3+} (~2.6 Å); however, this can be attributed to the different electronic configurations of Ce^{3+}, having one remaining 4f electron. Another ion with mentionable similarities to Ce^{IV} is Cm^{III},[55] which also coordinates nine water molecules in a tricapped trigonal-prismatic arrangement at a comparable mean ion−O distance (2.47−2.48 Å).

3.1.2. ADF. In Figure 3, the O−Ce−O ADF is shown. The ADF analysis clearly yields maxima in the regions of 70.5° and 136.5°, coinciding with the angular distribution found in a tricapped trigonal prism. A distinct minimum was not observed, but rather a valley between the two peaks, ranging from 84° to 121°, which can be attributed to multiple structural interconversions between the aforementioned trigonal prism and a capped square antiprism, was seen. Although the narrowness of the peaks reflects the strong solute−solvent interaction, the valley indicates intramolecular flexibility of the hydrate resulting from the structural reorganization taking place during the simulation. These findings are in agreement with the data found in the Ce−O ARD plot in Figure 5a).

3.1.3. Local-Density-Corrected Three-Body Distribution Functions. To further characterize the hydration beyond pairwise descriptions, the local-density-corrected three-body distribution functions $f^{(3)}_{O-X-O}(s,r,s)$ were calculated for the hydration spheres observed in the Ce−O RDF. For the first-shell O atoms, the function was evaluated up to a distance of 2.92 Å, and for the second sphere, the O atoms taken into account were located in a range from 3.95 to 5.26 Å. Another graph was plotted in order to account for the slight ordering of the water molecules between 5.94 and 7.44 Å, indicating a possible third shell. The shape of the local-density-corrected three-body distribution function $f^{(3)}_{O-X-O}(s,r,s)$ was compared to that of the O−O RDF of the pure solvent, enabling an investigation of the solute influence on the solvent structure. Figure 4 shows the local-density-corrected three-body distribu-

dx.doi.org/10.1021/ic300385s | Inorg. Chem. 2012, 51, 6746−6752

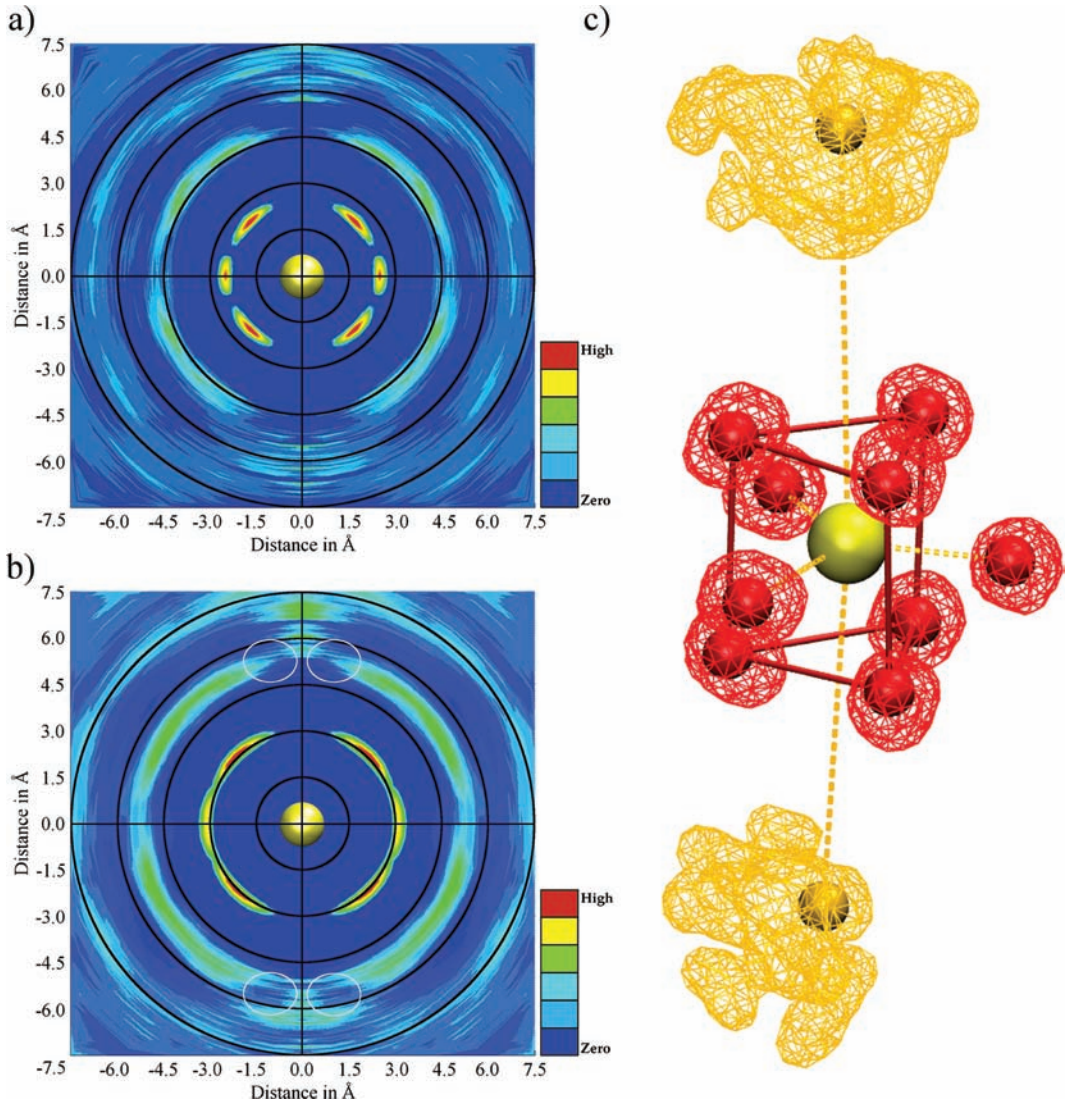

Figure 5. (a) Ce−O and (b) Ce−H ARDs. (c) Actual simulation screenshot at 5.0 ps resembling a tricapped trigonal-prismatic structure. Wireframes indicate the water localization over the last 5 ps of the simulation.

tion functions for the three hydration spheres as well as an O−O RDF of the pure solvent. The first-shell graph shows two distinct maxima at 2.85 and 4.65 Å, differing significantly from the O−O RDF, as expected clearly reflecting the stable structure of the first-shell hydrate. The graph of the second shell also suggests structural differences from the bulk, which appears reasonable given the strongly polarizing nature of the ion. When the third shell's graph is compared to that of the O−O RDF, a slight third-shell ordering of the water molecules can be observed for tetravalent cerium; for U^{4+},[15] Al^{3+},[41] and the recently investigated Zr^{4+},[48] weak third hydration spheres have also been identified. In the case of the larger U^{4+} ion,[8] this can be attributed to the presence of 5d electrons, whereas in the case of Al^{3+} and Zr^{4+}, the significantly smaller ionic radii[8] are responsible for their stronger polarizing character.

3.2. Dynamics. The stretching frequency of the Ce−O bond and its corresponding force constant were calculated from the simulation trajectory. Irrespective of the differences in the electronic structures of other ionic species,[48,26,56] the metal−O force constant (Table 1) serves as a sensitive tool to characterize the respective bond strengths. It can be concluded that the Ce−O bond (k_{ion-O} = 149 N m^{-1}) is weaker than the Zr−O, Be−O, and Al−O bonds. Because the published Be−O frequency has been scaled,[44,45,56] it has been unscaled prior to this comparison. Besides the comparison to QMCF-MD simulated ions, the Ce−O stretching frequency was compared to the frequency estimated by Sham et al.,[6] who used the upper limit value of 408 cm^{-1} of Ln^{3+} hydrated ions reported by Kanno and Hiraishi[7] to approximate the Ce−O stretching frequency. The value of 420 cm^{-1} derived from the QMCF-MD simulation agrees well with Sham's estimation.

The broad region of zero intensity in the Ce−O RDF between 2.92 and 3.84 Å indicates that no water exchanges between the first and second hydration spheres occurred during the simulation time of 10 ps. The nonzero minima between the second and third shells as well as between the third shell and bulk suggest that numerous water exchanges took place. Table 2 displays the second-shell MRTs and R_{ex} values computed with a direct method[42] in comparison to other QMCF-MD simulations[15,48,26,56] and pure water.[57] Because the second-shell MRT of 6.0 ps is a multiple of the value for pure water,[57] a strong Ce^{4+} structure-forming activity at least up to the second shell is evident. Al^{3+} [26] shows a much longer MRT than Ce^{4+}, which can be attributed to stronger hydrogen-bond formation

dx.doi.org/10.1021/ic300385s | Inorg. Chem. 2012, 51, 6746−6752

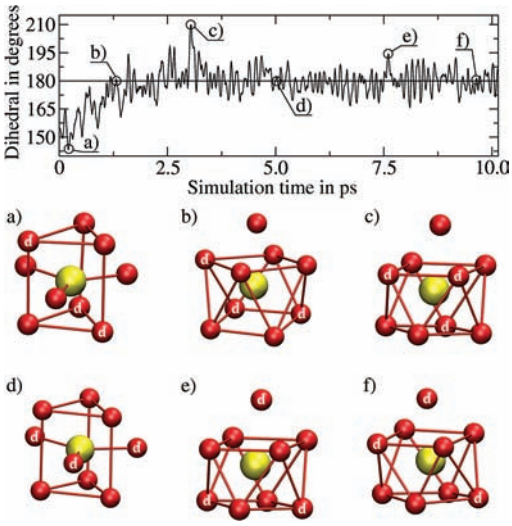

Figure 6. Top: Illustration of a dihedral angle defined by the O atoms denoted with "d" and the central ion. Screenshots: (a) Tricapped trigonal-prismatic structure at 0.2 ps. (b) Reordering of the O atoms, forming a capped square antiprism at 1.3 ps. (c) Reestablishment of the antiprismatic structure at 3.0 ps. (d) Conversion of the structure to a differently arranged tricapped trigonal prism at 5.0 ps. (e) Formation of a capped square antiprism at 7.6 ps. (f) Re-formation of the capped square antiprism at 9.6 ps.

between the first and second shells in the case of Al^{3+}. The smaller Be^{2+} [56] ion with its lower charge density outside its first hydration sphere shows a shorter MRT than Ce^{4+}. In contrast, U^{4+} shows a longer MRT,[15] indicating stronger structure-forming ability, which can be attributed to the bond-contributing 5d electrons.[58] The Zr^{4+} QMCF-MD simulation[48] yielded a MRT of 5.5 ps and a second-shell coordination number of 17.8, attesting to dynamical similarities with Ce^{4+}. When the R_{ex} values are compared, the prominent second-shell stability of Al^{3+} [26] appears evident. U^{4+} [15] and Zr^{4+} [48] showed similarities with Ce^{4+} in terms of exchange rate properties. Second-shell water ligand exchanges in the U^{4+} [15] QMCF-MD simulation tend to be less frequent than those in the case of Ce^{4+}, but fewer attempts are required to achieve lasting ligand exchanges.

Parts a and b of Figure 5 depict the Ce−O and Ce−H ARDs, evaluated over the last 5 ps of the simulation trajectory. The underlying geometry is shown in Figure 5c, where the water localization is illustrated by wireframe volume maps. The bonds are to be understood as fictive in order to demonstrate the underlying geometry of the first hydration shell at an actual simulation step (5.0 ps; tricapped trigonal-prismatic structure). In order to analyze the distribution of the water molecules, spatial distributions of the O atoms have been computed after alignment of the trajectory with respect to the first hydration shell. To illustrate distortions of the previously defined tricapped trigonal-prismatic mean structure, wireframe illustrations obtained with VMD's VolMap tool[59] are shown in Figure 5c. Besides the ordering of the water molecules in the first hydration sphere, the ARD plot shows both the second and third hydration shells as well. Interestingly, no water molecules are located in the axial position up to a distance of 5.3 Å coinciding with the beginning of the third shell. The respective water molecules (their O atoms are illustrated in orange in Figure 5c) are stabilized by hydrogen bonds formed with near-axial second-shell water molecules; the H atoms liable for the stabilization are shown in the corresponding region in the Ce−H ARD (Figure 5b, white circles).

The system's repetitive alteration between two hydration structures (tricapped trigonal-prismatic and capped square-antiprismatic structures) was investigated by monitoring the dihedral angles observed between planes defined by first-shell O atoms and the Ce^{4+} ion. Exemplarily, for the numerous and rapidly occurring pseudorotations resulting in first-shell structural changes, one dihedral angle was plotted over the 10 ps of the sampling trajectory. This dihedral angle was defined between the central ion and the three cap O atoms of a tricapped trigonal-prismatic structure observed during the simulation's sampling trajectory. Figure 6 shows, besides the time evolution of this particular dihedral angle, six first-shell hydration structures of interest.

4. CONCLUSION

This work presents the first quantum-mechanical simulation study of the tetravalent Ce ion in aqueous solution. The hydrated Ce ion proved very stable at ambient conditions within the relatively short simulation time frame; even at elevated temperature, no hydrolysis reactions were observed in contrast to other ions.[60] Therefore, besides U^{4+},[15] Zr^{4+},[48] and Th^{4+},[51−53] Ce^{4+} is one of the few stable tetravalent ions in aqueous solution. This QM approach should prove valuable for the interpretation of future experiments. The interesting solvent coordination served as a good example to prove the usefulness of analytical tools like the angular-radial distribution function and the local-density-corrected three-body distribution function. The excellent agreement of the QMCF-MD simulation with experimental results once again proves the quality of this methodology to investigate the structural and dynamical properties of solvated ions. The observation of structural shifts between the two predominant 9-fold-coordinated geometries indicates another advantage of a theoretical treatment compared to experimental approaches, where a detailed analysis of such ultrafast dynamic processes is still not feasible.

■ ASSOCIATED CONTENT

Ⓢ Supporting Information

HF, MP/2, and coupled-cluster optimized ion−water binding energies. This material is available free of charge via the Internet at http://pubs.acs.org.

■ AUTHOR INFORMATION

Corresponding Author

*E-mail: t.hofer@uibk.ac.at. Tel.: +43-512-507-57102. Fax: +43-512-507-57199.

Notes

The authors declare no competing financial interest.

■ ACKNOWLEDGMENTS

Financial support for this work from the Austrian Science Fund (FWF) is gratefully acknowledged.

■ REFERENCES

(1) Lide, D. R. *Handbook of Chemistry and Physics*; CRC Press: Boca Raton, FL, 2000.

(2) Macedo, A. G.; Fernandes, S. E.; Valente, A. A.; Ferreira, R. A.; Carlos, L. D.; Rocha, J. *Molecules* **Feb 2010**, *15* (2), 747−765.

(3) Takeda, N.; Irisawa, M.; Imai, T.; Yashiro, M.; Komiyama, M. *Nucleic Acids Symp. Ser.* **1995**, *34*, 207−208.

(4) Gao, P.; Kang, Z.; Fu, W.; Wang, W.; Bai, X.; Wang, E. *J. Am. Chem. Soc.* **2010**, *132* (12), 4197−4201.
(5) Solera, J. A.; García, J.; Proietti, M. G. *Phys. Rev. B* **1995**, *51* (5), 2678−2686.
(6) Sham, T. K. *Phys. Rev. B* **1989**, *40* (9), 6045−6051.
(7) Kanno, H.; Hiraishi, J. *J. Phys. Chem.* **1984**, *88* (13), 2787−2792.
(8) Shannon, R. D. *Acta Crystallogr.* **1976**, *32* (5), 751−767.
(9) Beattie, J. K.; Best, S. P.; Skelton, B. W.; White, A. H. *J. Chem. Soc., Dalton Trans.* **1981**, *10*, 2105−2111.
(10) Stillinger, F. H.; Rahman, A. *J. Chem. Phys.* **1978**, *68* (2), 666−670.
(11) Bopp, P.; Janscó, G.; Heinzinger, K. *Chem. Phys. Lett.* **1983**, *98* (2), 129−133.
(12) Moin, S. T.; Hofer, T. S.; Pribil, A. B.; Randolf, B. R.; Rode, B. M. *Inorg. Chem.* **2010**, *49*, 5101−5106.
(13) Kritayakornupong, C.; Vchirawongkwin, V.; Rode, B. M. *J. Comput. Chem.* **2010**, *31*, 1785−1792.
(14) Bhattacharjee, A.; Hofer, T. S.; Pribil, A. B.; Randolf, B. R.; Lim, L. H.; Lichtenberger, A. F.; Rode, B. M. *J. Phys. Chem. B* **2009**, *113*, 13007−13013.
(15) Frick, R. J.; Pribil, A. B.; Hofer, T. S.; Randolf, B. R.; Bhattacharjee, A.; Rode, B. M. *Inorg. Chem.* **2009**, *48*, 3993−4002.
(16) Vchirawongkwin, V.; Rode, B. M.; Persson, I. *J. Phys. Chem. B* **2007**, *111*, 4150−4155.
(17) Hofer, T. S.; Pribil, A. B.; Randolf, B. R.; Rode, B. M. In Combining Quantum Mechanics and Molecular Mechanics. Some Recent Progresses in QM/MM Methods. *Advances in Quantum Chemistry*; Sabin, J. R., Brandas, E., Eds.; Academic Press: New York, 2010; Vol. *59*, pp 213−246.
(18) Hofer, T. S.; Rode, B. M.; Pribil, A. B.; Randolf, B. R. In Theoretical and Computational Inorganic Chemistry. *Advances in Inorganic Chemistry*; van Eldik, R., Harvey, J., Eds.; Academic Press: New York, 2010; Vol. *62*, pp 143−175.
(19) Rode, B. M.; Hofer, T. S.; Randolf, B. R.; Schwenk, C. F.; Xenides, D.; Vchirawongkwin, V. *Theor. Chem. Acc.* **2006**, *115*, 77−85.
(20) Field, M. J.; Bash, P. A.; Karplus, M. *J. Comput. Chem.* **1990**, *11* (6), 700−733.
(21) Bakowies, D.; Thiel, W. *J. Phys. Chem.* **1996**, *100* (25), 10580−10594.
(22) Svensson, M.; Humbel, S.; Froese, R. D. J.; Matsubara, T.; Sieber, S.; Morokuma, K. *J. Phys. Chem.* **1996**, *100* (50), 19357−19363.
(23) Chung, L. W.; Hirao, H.; Li, X.; Morokuma, K. *WIREs Comput. Mol. Sci.* **2012**, *2* (2), 327−350.
(24) Mulliken, R. S. *J. Chem. Phys.* **1955**, *23* (10), 1833−1840.
(25) Mulliken, R. S. *J. Chem. Phys.* **1955**, *23* (10), 1841−1846.
(26) Hofer, T. S.; Randolf, B. R.; Rode, B. M. *J. Phys. Chem. B* **2008**, *112*, 11726−11733.
(27) Reed, A. E.; Weinstock, R. B.; Weinhold, F. *J. Chem. Phys.* **1985**, *83* (2), 735−746.
(28) Lowdin, P.-O. *J. Chem. Phys.* **1950**, *18* (3), 365−375.
(29) Dunning, T. H., Jr. *J. Chem. Phys.* **1970**, *53*, 2823.
(30) Roos, B. O.; Lindh, R.; Malmqvist, P.; Veryazov, V.; Widmark, P. O.; Borin, A. C. *J. Phys. Chem. A* **2008**, *112* (45), 11431−11435.
(31) Cundari, T. R.; Stevens, W. J. *J. Chem. Phys.* **1993**, *98* (7), 5555−5565.
(32) Huzinaga, S.; Miguel, B. *Chem. Phys. Lett.* **1990**, *175* (4), 289−291.
(33) Ying, J.; Mathers, C.; Leung, K.; Pritchard, H.; Winstead, C.; McKoy, V. *Chem. Phys. Lett.* **1993**, *212* (3−4), 289−297.
(34) Dolg, M.; Cao, X. *J. Chem. Phys.* **2012**.
(35) Dolg, M.; Stoll, H.; Preuss, H.; Pitzer, R. M. *J. Phys. Chem.* **1993**, *97* (22), 5852−5859.
(36) Feller, D. *J. Comput. Chem.* **1996**, *17* (13), 1571−1586.
(37) Schuchardt, K. L.; Didier, B. T.; Elsethagen, T.; Sun, L.; Gurumoorthi, V.; Chase, J.; Li, J.; Windus, T. L. *J. Chem. Inf. Model.* **2007**, *47* (3), 1045−1052.
(38) Frisch, M. J.; Trucks, G. W.; Schlegel, H. B.; Scuseria, G. E.; Robb, M. A.; Cheeseman, J. R.; Scalmani, G.; Barone, V.; Mennucci, B.; Petersson, G. A.; Nakatsuji, H.; Caricato, M.; Li, X.; Hratchian, H. P.; Izmaylov, A. F.; Bloino, J.; Zheng, G.; Sonnenberg, J. L.; Hada, M.; Ehara, M.; Toyota, K.; Fukuda, R.; Hasegawa, J.; Ishida, M.; Nakajima, T.; Honda, Y.; Kitao, O.; Nakai, H.; Vreven, T.; Montgomery, J. A., Jr.; Peralta, J. E.; Ogliaro, F.; Bearpark, M.; Heyd, J. J.; Brothers, E.; Kudin, K. N.; Staroverov, V. N.; Kobayashi, R.; Normand, J.; Raghavachari, K.; Rendell, A.; Burant, J. C.; Iyengar, S. S.; Tomasi, J.; Cossi, M.; Rega, N.; Millam, J. M.; Klene, M.; Knox, J. E.; Cross, J. B.; Bakken, V.; Adamo, C.; Jaramillo, J.; Gomperts, R.; Stratmann, R. E.; Yazyev, O.; Austin, A. J.; Cammi, R.; Pomelli, C.; Ochterski, J. W.; Martin, R. L.; Morokuma, K.; Zakrzewski, V. G.; Voth, G. A.; Salvador, P.; Dannenberg, J. J.; Dapprich, S.; Daniels, A. D.; Farkas; Foresman, J. B.; Ortiz, J. V.; Cioslowski, J.; Fox, D. J. *Gaussian 09*, revision A.02; Gaussian, Inc.: Wallingford, CT, 2009.
(39) Ross, R.; Ermler, W.; Das, S. Unpublished.
(40) Kuta, J.; Clark, A. E. *Inorg. Chem.* **2010**, *49* (17), 7808−7817.
(41) Bhattacharjee, A.; Hofer, T. S.; Rode, B. M. *Phys. Chem. Chem. Phys.* **2008**, *10*, 6653−6657.
(42) Hofer, T. S.; Tran, H. T.; Schwenk, C. F.; Rode, B. M. *J. Comput. Chem.* **2004**, *25* (2), 211−217.
(43) Rode, B. M.; Schwenk, C.; Hofer, T.; Randolf, B. *Coord. Chem. Rev.* **2005**, *249* (24), 2993−3006.
(44) Scott, A. P.; Radom, L. *J. Phys. Chem.* **1996**, *100* (41), 16502−16513.
(45) DeFrees, D. J.; McLean, A. D. *J. Chem. Phys.* **1985**, *82*, 333−341.
(46) Berendsen, H. J. C.; Postma, J. P. M.; van Gunsteren, W. F.; DiNola, A.; Haak, J. R. *J. Phys. Chem.* **1984**, *81*, 3684−3690.
(47) Adams, D. J.; Adams, E. M.; Hills, G. *J. Mol. Phys.* **1979**, *38* (2), 387−400.
(48) Messner, C. B.; Hofer, T. S.; Randolf, B. R.; Rode, B. M. *Phys. Chem. Chem. Phys.* **2011**, *13*, 224−229.
(49) Yang, T.; Tsushima, S.; Suzuki, A. *J. Phys. Chem. A* **2001**, *105* (45), 10439−10445.
(50) Réal, F.; Trumm, M.; Vallet, V.; Schimmelpfennig, B.; Masella, M.; Flament, J.-P. *J. Phys. Chem. B* **2010**, *114* (48), 15913−15924.
(51) Moll, H.; Denecke, M. A.; Jalilehvand, F.; Sandstrom, M.; Grenthe, I. *Inorg. Chem.* **1999**, *38* (8), 1795−1799.
(52) Sandström, M.; Persson, I.; Jalilehvand, F.; Lindquist-Reis, P.; Spångberg, D.; Hermansson, K. *J. Synchrotron Radiat.* **2001**, *8* (2), 657−659.
(53) Torapava, N.; Persson, I.; Eriksson, L.; Lundberg, D. *Inorg. Chem.* **2009**, *48* (24), 11712−11723.
(54) Dinescu, A.; Clark, A. E. *J. Phys. Chem. A* **2008**, *112* (44), 11198−11206.
(55) Yang, T.; Bursten, B. E. *Inorg. Chem.* **2006**, *45* (14), 5291−5301.
(56) Azam, S. S.; Hofer, T. S.; Bhattacharjee, A.; Lim, L. H.; Pribil, A. B.; Randolf, B. R.; Rode, B. M. *J. Phys. Chem. B* **2009**, *113*, 9289−9295.
(57) Xenides, D.; Randolf, B. R.; Rode, B. M. *J. Chem. Phys.* **2005**, *122*, 4506.
(58) Holleman, A. F.; Wiberg, N. *Inorganic Chemistry*; Academic Press Inc.: New York, 2001.
(59) Humphrey, W.; Dalke, A.; Schulten, K. *J. Mol. Graphics* **1996**, *14*, 33−38.
(60) Bhattacharjee, A.; Hofer, T. S.; Pribil, A. B.; Randolf, B. R.; Rode, B. M. *Chem. Phys. Lett.* **2009**, *473* (1−3), 176−178.